stellarator news

Published by Fusion Energy Division, Oak Ridge National Laboratory
Building 9201-2; P.O. Box 2009; Oak Ridge, TN 37831-8071, USA
Editor: James A. Rome Issue #32 March 1994
E-Mail: jar@ornl.gov Phone: (615) 574-1306

Around the Labs

High beta experiments in CHS

For three experimental run weeks last September, experiments were conducted in the Compact Helical System (CHS) for the purpose of achieving high beta plasmas in a helical system. Two hydrogen neutral beam injectors were used in a balanced tangential injection configuration. The neutral beams had been conditioned in advance of the experiments. Both beam injectors worked at full performance during the entire experimental period. NBI-1 was used for coinjection with 1.1 MW of port-through power at 40 keV energy and NBI-2 for counterinjection with 0.8 MW of port-through power at 36 keV. The optimum magnetic field strength (B_{av} = 0.57 T) was selected for achieving the highest beta level. The ability to choose the magnetic field strength is a benefit of target plasma production based on nonresonant ICRF heating with the Nagoya Type-III antenna.

The average equilibrium beta value of 2.1% (including tangential beam contribution) was obtained with 1.4 MW absorbed power. Figure 1 shows the time behavior of plasma parameters in one of highest beta discharges. Strong gas puffing (hydrogen) was turned off when the plasma energy started to decrease because of the confinement degradation at the high-density limit. The diamagnetic beta value increased during the decreasing phase of the density, which is denoted as the reheat mode. The peak diamagnetic beta value was 2.0% with the line-averaged density $n_e = 6.5 \times 10^{19}$ m^{-3} and the average magnetic field was 0.57 T.

Titanium gettering was used for the wall conditioning. The repetitive use of titanium gettering increased the practical density limit day by day, which led to an increase of beta. Figure 2 shows the relation between the diamagnetic beta values and the line-averaged densities.

Open circles are maximum beta values achieved during the gas puffing and closed circles are peak beta values after turning off the gas puffing. The betas with the gas puffing are almost in proportion to the corresponding density. The reheat mode gave substantial improvement of beta for high-density discharges. Because high-beta discharges are made at the limits of operational parameters (low magnetic field and high density), the global energy confinement time is lower than predicted from the Large Helical Device (LHD) confinement scaling. The reheat mode operation gave a 25% improvement of confinement to these high density operations.

Preliminary experiments for evaluating the effect of wall boronization had been made in CHS in advance of the high-beta experiments. Although the favorable effects of boronization were observed in a number of aspects, titanium gettering was finally selected for the wall conditioning of high-beta experiments mainly because the technical preparation for a reliable procedure of boronization had not yet been fully established.

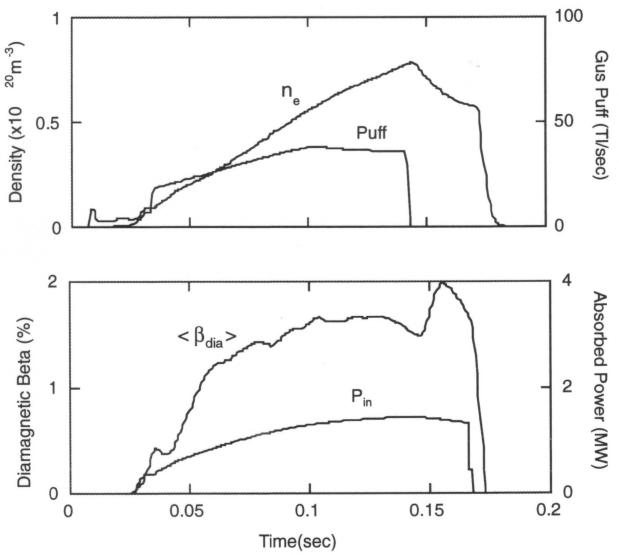

Fig. 1. Time behavior of the high-beta discharge. Line averaged density, gas puffing rate, diamagnetic average beta, and NBI absorbed power are shown.

For the beta range $\beta \leq 2$ %, no significant degradation of global confinement which is attributed to the plasma beta has been observed. The magnetic fluctuations were measured with 16 magnetic probes installed in both toroidal and poloidal arrays. The dependence of detected magnetic fluctuations on the average betas are shown in Fig. 3. Fig. 3(a) shows the fluctuations averaged over 3- to 100-kHz spectrum. This signal is from the probe which is located at a position (top side of the plasma) that is insensitive to the plasma (horizontal) movement caused by finite beta effects. The fluctuation level increases almost in proportion to the β value for β up to 1%, but saturates at higher values of β. Fig. 3(b) show the dependence of dominant coherent mode amplitudes on the plasma beta. The m=2/n=1 mode increased more rapidly for the beta range $\beta < 1$%, whereas it decreases for higher beta values and finally disappears for $\beta > 1.3$%. The 1/1 mode appears for $\beta >$ 0.5%, and it becomes the largest coherent mode for $\beta >$ 1.3 %.

The plasma position control in CHS has a large effect on MHD stability. The outward-shifted configuration has a strong magnetic well in its vacuum field. However the global confinement database of NBI discharges shows better confinement for the inward shifted case. Since the limitation of beta is due to confinement in the present experimental conditions, the inward shifted configuration was used in high-beta experiments. Although the Mercier stability criterion shows an unstable region ($r/a < 0.5$) for the low-beta configuration, the large Shafranov shift (40% of the minor radius) digs a magnetic well in high-beta discharges which yields complete Mercier stability over the whole radius.

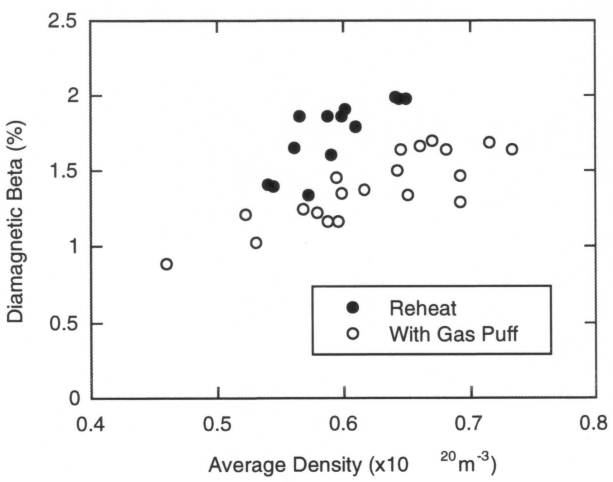

Fig. 2. Diamagnetic average beta and line-averaged density. Open circles are for maximum beta values during gas puffing, and closed circles are for peak beta values in reheat mode.

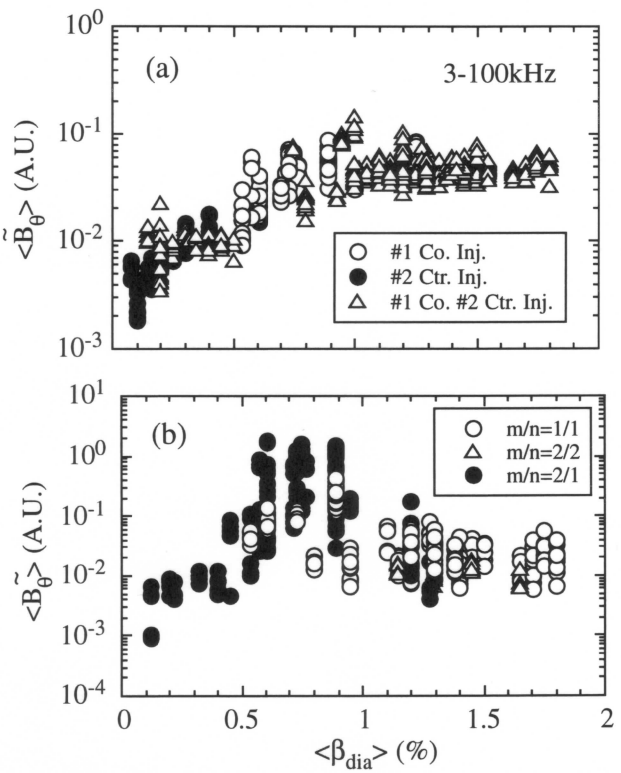

Fig. 3. Dependence of (a) averaged magnetic fluctuations and (b) coherent mode amplitudes on diamagnetic beta.

The plasma position moves 0.8 cm outward when the plasma beta reaches 2%. Because the plasma boundary of the inward-shifted configuration is determined by the inboard-side vacuum chamber wall, this movement causes the plasma volume to increase. The formation of a self-induced magnetic well is the combined effect of such outward shift of magnetic surfaces and the Shafranov shift. Volume expansion also causes the normalized radius (r/a) of the magnetic surface with $\iota = 1$ to change from 1.0 to 0.93.

Dynamic poloidal field control during the discharge was implemented in order to fix the plasma boundary position when the plasma beta increased. This method is also technically useful to fix the plasma boundary during a high-beta discharge to prevent interference between the plasma boundary and the objects in the plasma periphery such as the limiters or divertors. The position of the plasma boundary was measured by visible ultraviolet (VUV) profile measurement with a rotating mirror, and the density profile was measured using a lithium beam probe at the plasma edge. Figure 4 shows the temporal change of the edge density profiles measured by a lithium probe for (a) no poloidal field control case and (b) poloidal field control case. The total plasma energies were almost the same for both cases,

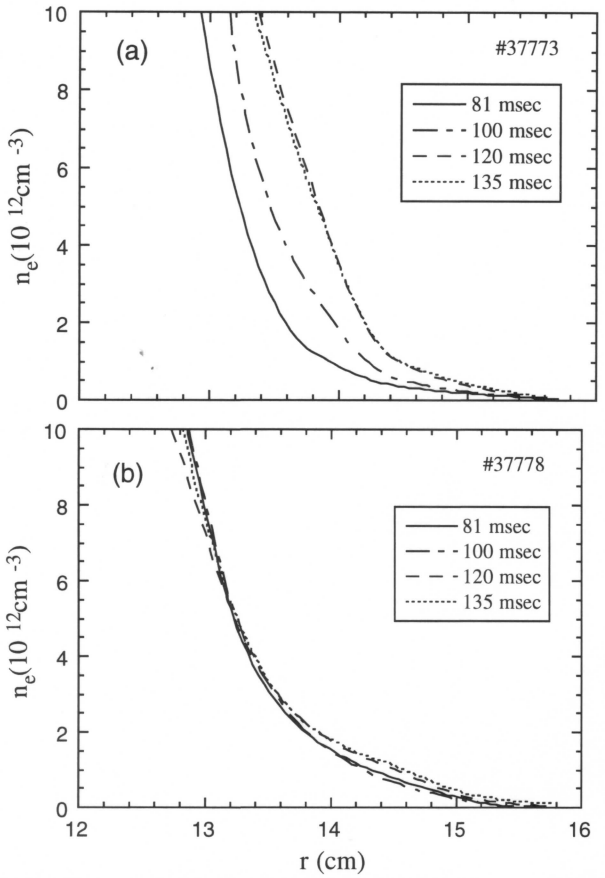

Fig. 4. Evolution of edge density profiles for (a) no poloidal field control and (b) dynamic poloidal field control.

but an increase of the average beta was obtained for the discharges with poloidal field control. The Mirnov signals in poloidal field control discharges were roughly 1.5 times larger when compared with normal discharges.

Shoichi Okamura for CHS group
National Institute for Fusion Science
Nagoya 464-01, Japan
E-mail : okamura@nifs.ac.jp

Resonant magnetic field structures and radial plasma parameter profiles at the edge of W7-AS

In W7-AS, large "natural" boundary magnetic islands offer the potential of open divertor operation. They belong to the major resonances at local rational values $\iota = 5/m$. As a pre-study in this context, the impact of such resonances on the edge plasma parameter profiles was investigated by fast reciprocating Langmuir probes for various configurations in the edge rotational transform range $\iota_a = 0.45$ to 0.6, including the 5/11, 5/10 and 5/9 resonances.

The discharge conditions were chosen to keep the configurations close to the vacuum field: currentless, flat-top ECRH discharges with $P_{heat} = 160$ kW and $\langle n_e \rangle = 1\times10^{19}m^{-3}$. The two main limiters were fixed at their outermost positions. Langmuir probes were placed close to the triangular plasma cross section at the toroidal angle $\varphi = 72°$. One probe was in the vicinity of the outboard tip (X-point position for all resonant cases), with another one slightly below the midplane of the configuration towards the bottom part of the magnetic topology. In the case of a major resonance, this probe intersects boundary magnetic islands (or their remnants in the case of an open edge topology) at some poloidal distance of the O-point. The edge plasma parameter profiles show strong, quasiperiodical variations with ι_a, which are clearly correlated to the separatrix positions calculated by field line tracing. Figure 1 shows examples of typical profiles measured by the second probe for two conditions, case (a) at $\iota_a = 0.549$ and case (b) at $\iota_a = 0.529$, respectively. In case a), both the ion saturation current I_s and the electron temperature T_e profiles show pronounced flat regions. The connection lengths L_c are derived from field line tracing between the probe tip and boundaries, the two limiters of W7-AS, various in-vessel objects, and the torus wall. The probe intersects part of the 5/9 resonance in case (a), where the limiters introduce finite, but rather long connection lengths. In case (b), the island cannot be formed due to the short connection lengths introduced by the in-vessel objects of W7-AS, and the profiles of I_s and T_e decrease continuously. The space potential has a flat region inside the resonance region in case (a); in case (b) there is a sharply pronounced maximum at the calculated separatrix position.

By varying ι_a, these profile types return quasi-periodically corresponding to the occurrence and radial shift of the $5/m$ separatrix in very good accordance with vac-

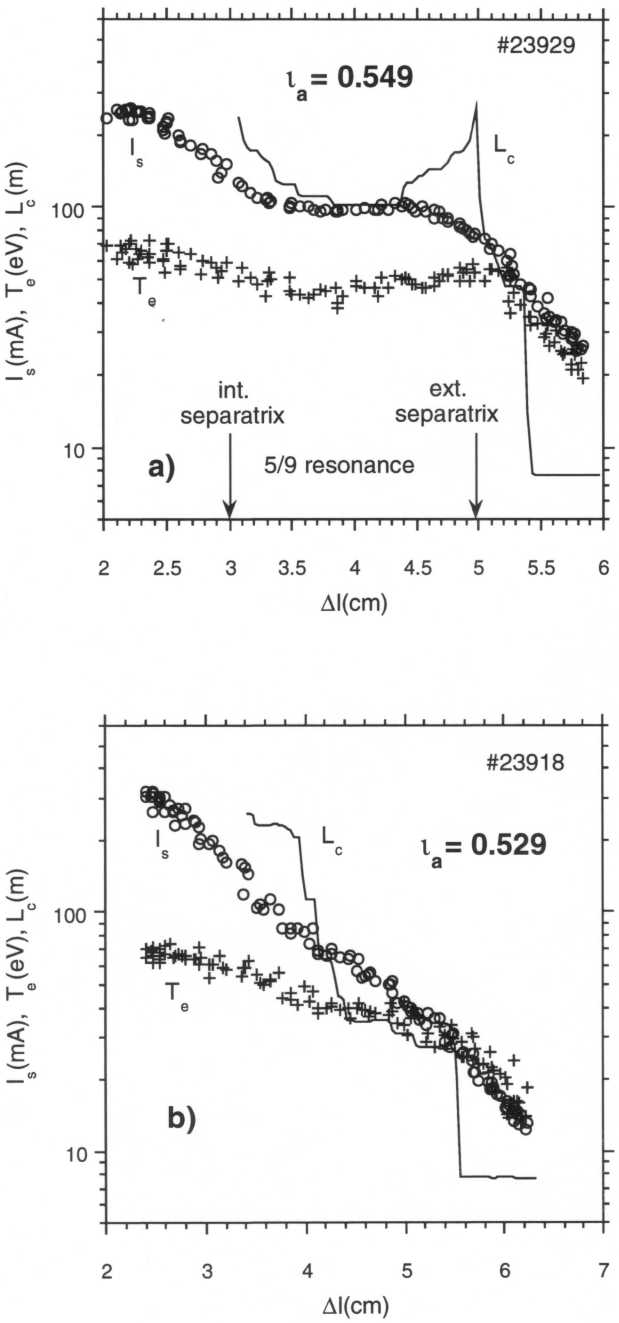

Fig. 1. Radial profiles of the ion saturation current I_s and electron temperature T_e from Langmuir probe measurements for low-beta currentless ECRH discharges, as well as connection lengths L_c derived from field line calculations. Edge profile broadening by the 5/9 resonance is present for case (a).

uum field calculations. We conclude that the $5/m$ resonances are a reality in the W7-AS edge structure with respect to particle and energy transport. In cases with sufficiently long L_c, they introduce a radial short circuit by strong parallel components. Most of the profile shoulders we found can be explained in this way. The identified separatrix positions agree very well with vacuum field calculations, both spatially and with respect to the ι scale. From radial density profiles of type (b), particle transport coefficients (averaged in the parallel direction) were zero-dimensionally estimated for $\iota_a = 0.34$ (limiter-bounded) and 0.53 (separatrix bounded). They show a unique scaling with the inverse of the plasma density at the last closed magnetic surface. For low to moderate densities and for two poloidal probe positions, no indications of an ι-dependency or poloidal asymmetry were found within the limits of the simple model of edge transport. More information of these studies will be presented at the forthcoming PSI conference.

P. Grigull and G. Herre,
IPP Garching, Germany
Phone: 0049-89-3299-1619
FAX: 0049-89-3299-2584
E-Mail PEG @ IBMA.IPP-GARCHING.MPG.DE

Plasma shaping by quadrupole field control in CHS

Neoclassical theory is necessarily mentioned in connection with experiments in helical systems because of the possibly significant effects of the various components of magnetic field ripple. A configurational study based on 3-D neoclassical theory indicates that the tailoring of helical ripples can control thermal conductivity and the geometrical factor for bootstrap current. We have investigated the transport behavior of ECRH plasmas over a wide range of magnetic configurations and compared the results with 3-D neoclassical theory.

The structure of the helical ripple can be controlled by the magnetic axis position R_{ax} (dipole field control) and/or plasma shaping k (quadrupole field control). In the magnetic axis scan, however, other important physical parameters such as the rotational transform ι, shear, magnetic well/hill, and the power deposition profile also change. Therefore, we have varied the plasma ellipticity by controlling the quadrupole component while maintaining other physical parameters (R_{ax}, ι, magnetic well/hill, and ECRH power deposition). Although a similar experiment has been done in the ATF torsatron, investigation of plasmas with a complex mixture of helical harmonics is possible in CHS because of its low aspect

ratio;and independent verification of the ATF results is important.

The experiment has been performed using the second harmonic ECRH (53 GHz, 150 kW) at $B_t = 0.95$ T. Thomson scattering measurement indicates typical central temperature of around 650 to 800 eV. Toroidal current up to 1.5 kA has been observed. The shot-by-shot scan has covered the toroidally averaged ellipticity of plasma shape k of 0.9 (vertically squeezed configuration, oblate) to 1.6 (vertically elongated configuration, prolate). The position of the magnetic axis is set at 0.92 m, where the excursion of the position of magnetic axis is least, and hence central ECR heating is expected to be the most efficient. The plasma minor radius is fixed at 0.165 m by means of two movable limiters located on the high field side and 180° apart in the toroidal direction. The plasma boundary is well defined by these limiters or by the inner wall of the vacuum vessel. The focused wave of electron cyclotron resonant heating (ECRH) is launched into the plasma center perpendicularly to the magnetic field line. The line-averaged electron density is also kept at 8×10^{18} m^{-3}, which is below the cutoff density of ECRH. This experimental setup means that the global characteristic parameters that appear in the scaling study are kept constant during the scan.

Impurity content affects the collisionality significantly. Subsequently, changes in Z_{eff} can play an important role in the interpretation of the experimental results. Unfortunately, a direct measurement of Z_{eff} with the bremsstrahlung diagnostic did not provide a reliable value for the present experiment since the operational density is quite low. However, Z_{eff} does not seem to change significantly because the total radiation power changes only from 26 kW for $k = 0.9$ to 20 kW for $k = 1.6$.

Figure 1 shows an example of temporal behavior of plasma parameters. The direction of positive current is that of intrinsic rotational transform, which does not contradict the picture of bootstrap current. When the magnetic field is reversed, the same amount of current with the opposite direction is observed. This indicates that the current is not driven directly by the ECRH. Since the self-inductance of the toroidal plasma loop is a few millihenrys and the applied poloidal flux is less than 5×10^{-5} Vs during discharges, ohmically induced current should be less than 100 A. Therefore, the observed toroidal current can be bootstrap current. Discharge duration is limited to 80 ms due to the capability of the ECRH system, whereas the confinement time and resistive current diffusion time are about 3 ms and 100 ms, respectively. Since bootstrap current flows preferentially in the outer region of the plasma where there is a large pressure gradient, the current relaxation can occur in the short time scale. The pulse duration is long enough to establish thermal equilibrium but not quite long enough for realization of a steady-state current distribution. Indeed, the observed toroidal current has not shown clear evidence of saturation even though the kinetic profiles should have reached steady-state.

The experimental observation of energy confinement time and toroidal current for the plasma shaping scan are plotted in Fig. 2. Here the experimental data for the toroidal current are taken at the end of the ECRH pulse. A rough analysis suggests that neoclassical theory predicts good confinement for the oblate configuration and bad confinement for the prolate configuration. However, the energy confinement time does not change significantly over the scan, which suggests that global confinement is determined by a mechanism other than the neoclassical transport. This picture is consistent with the results of local transport analysis, as will be mentioned later.

On the other hand, the toroidal current shows a clear dependence on the plasma ellipticity. The amount of current decreases with the plasma elongation for k_1. This is consistent with a simple argument that the oblate configuration is good for the confinement of trapped parti-

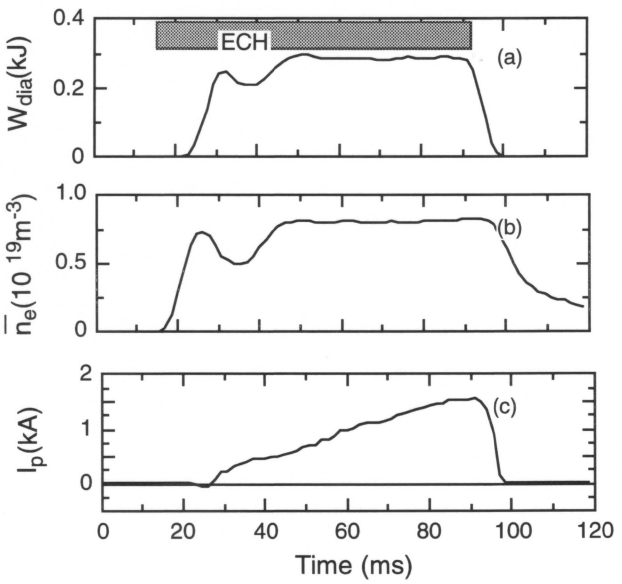

Fig. 1. Typical temporal behavior of ECRH plasma. (a) Total stored energy measured by a diamagnetic loop. (b) Line averaged electron density. (c) Toroidal current.

cles and the prolate is bad. The estimated neoclassical bootstrap current together with the experimental profile data are also plotted in Fig. 2. For the neoclassical calculation, we have shown bands when we assume Z_{eff}. The assumption of $Z_{eff} = 1$ gives the lower limit of theoretical value and that of $Z_{eff} = 3$ gives the upper limit. The experimental observation can be explained by neoclassical theory, although the agreement cannot be blindly claimed in a quantitative sense because of the current has not reached a quasi-steady state.

It is possible to reverse the bootstrap current by using extreme plasma elongation, which has been already realized on ATF. We have also confirmed the reversal of the current itself when $k = 1.8$. In this case, however, the plasma is bounded by a separatrix and the minor radius is smaller (0.145 m) than the scanned plasmas reported in this article. We do not discuss this case here since the characteristics of the plasma are rather different.

The power balance is calculated by the 1-D profile analysis code PROCTR-MOD which can deal with the full 3-D geometry. We have investigated the dependence of the electron thermal conductivity on the plasma shaping effect (see Fig. 3). The value of the electron thermal conductivity at a half radius stays near the neoclassical estimate within the factor of 3. However, while the neoclassical theory indicates that electron thermal conductivity deteriorates with an increase in the ellipticity, the experimental result shows an opposite dependence. The evidence that the observed value is close to the neoclassical prediction is supposed to be a coincidence and not a correlation. This means a mechanism other than neoclassical plays a part in transport. The trend shown in Fig. 3 sets up a question about the argument that heat transport is neoclassical in the collisionless regime in helical plasmas.

We have investigated the response of the plasma by changing the structure of the magnetic ripples to enhance neoclassical transport. Recently, for neutral beam injection (NBI)-heated plasmas, the damping of toroidal rotation has been explained well by neoclassical viscous damping. The present experiment on bootstrap current also suggests that the transport parallel to the field line is neoclassical. However, transport perpendicular to the magnetic field line (thermal transport) does not look neoclassical, even in the collisionless regime. These observations are consistent with other experimental results in ATF as well as in tokamaks.

Neoclassical transport has been recognized to play a crucial role in the confinement of a reactor-grade collisionless plasmas in helical systems. The present experiment suggests that neoclassical theory is reliable for the prediction of bootstrap current but that thermal transport is not predictable using present neoclassical theory.

H. Yamada for the CHS group
National Institute for Fusion Science
Nagoya 464-01, Japan
Phone: +81-52-781-5111 ext.4599
FAX: +81-52-782-8493
Email: yamada@roprint.nifs.ac.jp

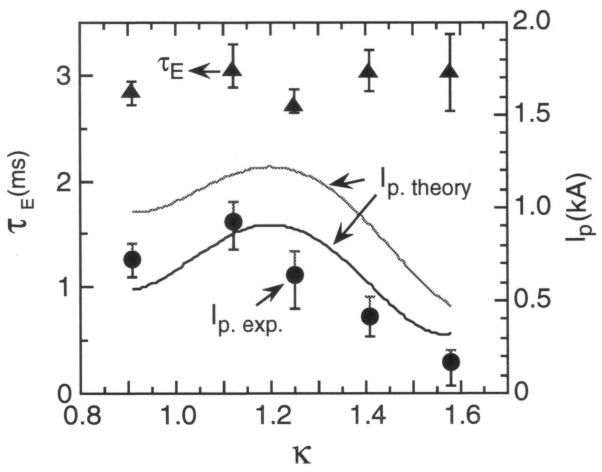

Fig. 2. Energy confinement time and toroidal current (filled circles) as a function of plasma ellipticity. Two curves for the bootstrap current estimated by the neoclassical theory with $Z_{eff} = 1$ (lower) and 3 (upper). Filled triangles show the stored energy in the experiment.

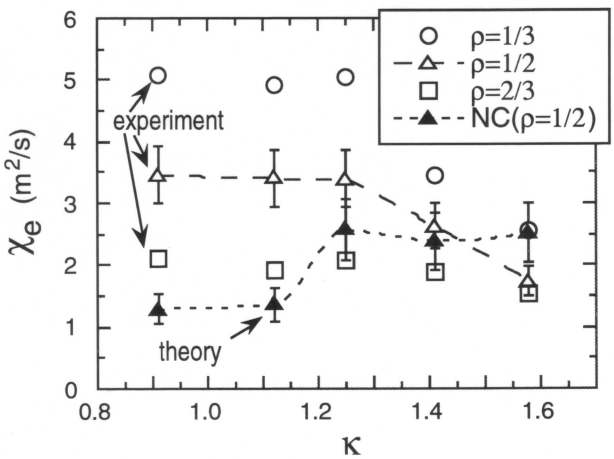

Fig. 3. Electron thermal conductivity as a function of plasma ellipticity. Open symbols show the experimental data at one third radius, half radius, and two-thirds radius. Solid symbols show the neoclassical prediction at half radius. The error bars come from the statistical error in the Thomson scattering diagnostics as well as from the assumption of Z_{eff}.

U.S. stellarator power plant study

The same group that studied the ARIES tokamak will spend this year applying the same tools to a stellarator power plant. The engineering aspects of the study will be guided by Farrokh Najmabadi (UCLA, UCSD) with help from industry. The physics input will be provided by a group coordinated by James Rome (ORNL).

The SPPS team had its first meeting in Oak Ridge, Tennessee at the beginning of January, and they met again on March 12 in Dallas, Texas before the Sherwood Theory Meeting. The first order of business was to select the best possible configuration for the study. Many options were discussed, but the choice quickly narrowed to two possibilities:

Modularization of a continuous helical torsatron

James Rome has devised an improved version of the symmotron modularization scheme. The key to this improvement is to drop the restriction that each module must be up/down symmetric. The optimum modularization scheme is shown in Fig. 1. The location of the windback was varied from $\theta = \pm 0°$ to $\theta = \pm 180°$. Two optima occurred at about 45° from the outside or from the inside. The outside location was chosen so that the windback can provide most or all of the required vertical field. A set of inner VF coils is required for shaping control. A key point to note is that the legs connecting the helix to the windbacks are perpendicular to the torus. This minimizes the field interaction with the plasma and preserves most of the plasma properties of the unmodularized configuration.

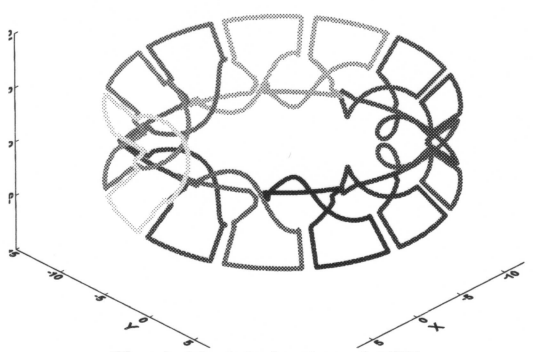

Fig. 1. Modularization of ATF.

Accordingly, since time and resources were limited, it was decided to modularize ATF. The resulting configuration (called MATF) has a 0.95-m intermodule gap for a 10-m major radius machine. In addition, the plasma-coil spacing provides the required 1.2-m gap.

Some advantages and disadvantages of the MATF configuration are listed in the following table:

Item	Advantage	Disadvantage
MHD	Second stability	$\beta > 5\%$ not needed
Transport	E-field heals thermal loss cone; easy ash removal	High neoclassical losses? Big loss cone for αs
Divertor	Could be outside coils; easier maintenance access	αs and thermals come out at different places
Coils	Easier to visualize; all modules identical; big access ports	Sharp bends
Other	Like ATF	Like ATF

Modular helias-like heliac (MHH)

The second configuration was devised by Paul Garabedian (NYU) and first was modularized by David Anderson (University of Wisconsin). The MHH was initially based upon a highly modulated heliac with a hard core and linked circular toroidal field coils. The physics properties were chosen to emulate the helias as much as possible. Because much of the rotational transform in MHH is produced by the helical excursion of the magnetic

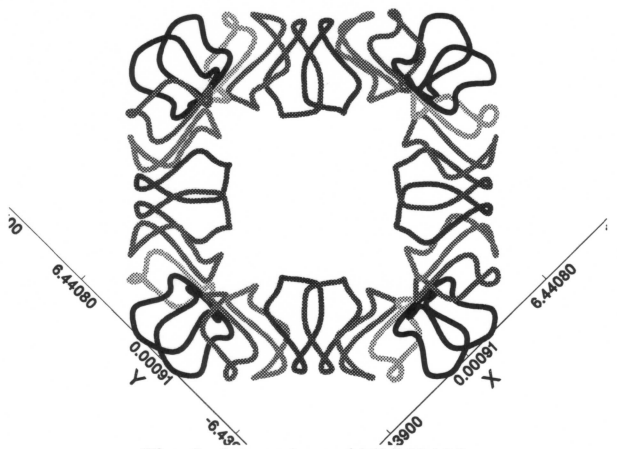

Fig. 2. A top view of MHH0103.

axis, the plasma-coil spacing is larger than that in W7-X for a given major radius. In a 14-m MHH, the plasma-coil gap is greater than 1.45 m everywhere. A picture of the configuration of January 3 (MHH0103) is shown in Fig. 2.

Some advantages and disadvantages of the MHH configuration are listed below:

Item	Advantage	Disadvantage
MHD	Stable to $<\beta> = 5\%$; J_{BS} small; ι independent of β.	High-n ballooning modes?
Transport	Quasi-helical	Ash accumulation
Divertor	Must be inside coils; access requires segment removal	αs and thermals come out at same place
Coils	Smaller size; 4 different coil types	Sharp bends; out-of-plane loads high; tight access between coils
Other	Like W7X; physics may be better than a tokamak	Divertor and blanket geometry difficult

At the January meeting, it was unanimously decided to use MHH as the basis for SPPS.

One of the biggest issues for MHH is how to manage the divertor. Using the NESCOIL code (Peter Merkel of IPP, Garching), it is possible to change the coil-winding surface while maintaining the same plasma configuration. In this way, the plasma-coil region can be made to be completely chaotic, to have islands in a chaotic sea, or to have islands surrounded by a good flux surface. The last-mentioned configuration is entirely analogous to the divertor geometry in a tokamak. Thus, if a good solution is developed for ITER, it can be applied (with some geometric complications) to the MHH as well.

Modification of 1-D transport code ASTRA for Wendelstein 7-X

Numerous problems arising in existing and planned stellarator experiments require a flexible transport code that is able to assess experimental results, test theoretical transport models, and make predictions. Such a code was recently adapted for stellarator tasks from the time- and radially-dependent code ASTRA. Originally, ASTRA (Automatic System for Transport Analysis) was a tokamak-oriented code created a few years ago [1] at the Kurchatov Institute for Atomic Energy, Moscow.

The stellarator version of ASTRA solves three flux-surface-averaged balance equations in a noncircular geometry, namely for the electron density n_e and for the electron and ion temperatures T_e and T_i. The radial profile of the rotational transform $\iota(r)$ is fixed.

Plasma transport properties are described by a transport matrix including nondiagonal elements, so the particle and heat fluxes are dependent on temperature and density gradients and on a radial electric field:

$$\Gamma_j = -D_1 n_j \left[\frac{n'_j}{n_j} + \frac{q_j \Phi'}{T_j} + \left(\frac{D_2}{D_1} - \frac{3}{2} \right) \left(\frac{T'_j}{T_j} \right) \right]$$

$$Q_j = D_2 n_j T_j \left[\frac{n'_j}{n_j} + \frac{q_j \Phi'}{T_j} + \left(\frac{D_3}{D_2} - \frac{3}{2} \right) \left(\frac{T'_j}{T_j} \right) \right]$$

where the subscript j denotes the particle species. At present, the species are restricted to electrons and hydrogen ions.

ASTRA is supplemented by a library which contains a numerous set of plasma physics formulae and expressions covering the most important needs of transport modeling, and the representation and analysis of calculated results. At present, this internal library in its stellarator-specific part contains the neoclassical coefficients derived by Beidler for Helias stellarators ,[2] Kovrizhnykh's coefficients for axially symmetric transport, [3] and anomalous electron thermal conductivity according to the ASDEX L-mode. Since the radial electric field also appears in the transport coefficients itself, the particle and heat fluxes depend on Φ' nonlinearly. The ambipolar electric field is calculated under the requirement of equality of the surface-averaged particle fluxes $\Gamma_e(r) = \Gamma_i(r)$.

The right parts of the energy balance equations contain common energy sinks and sources: bremsstrahlung, synchrotron and impurity radiation, energy losses on neutrals penetrating into the plasma from its boundary, energy exchange between plasma species, as well as

terms responsible for plasma heating. A model for the electron cyclotron heating with a second harmonic O-mode is available, where the power absorption depends on the electron temperature and density.

The code is well suited for the analysis and development of theoretical transport models using time-dependent experimental profiles as input. The principle of programming a task for an ASTRA calculation is to assemble a required plasma model from the library blocks and to set up appropriate boundary and initial conditions of the case of interest. The time dependence of values which are not calculated (for example the ECRH heating power) can be prescribed. Most of the problem variables characterizing the model and programmed control parameters can be interactively managed and changed during the calculation.

An example of various calculations carried out by ASTRA for Wendelstein 7-X is given in the accompanying figures. The results fit well to those made earlier using the Garching version of the transport code TEMPL if the same plasma model is used, see [4]. Owing to its flexibility and speed, ASTRA is especially suitable for scenario assessments, planning of experiments, reactor studies and, eventually, for modeling the L–H transition.

Nikolai Karulin
IPP Garching, Germany
Phone: 0049-89-3299-1498
FAX: 0049-89-3299-2579
E-mail: NIK@IBMA.IPP-GARCHING.MPG.DE

References

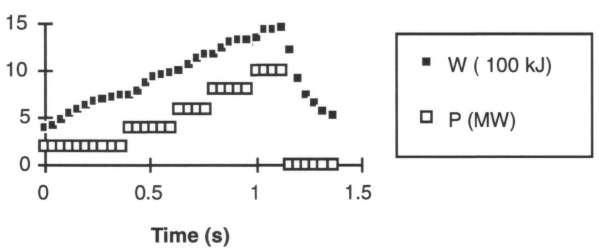

Fig. 1. Time development of the stored plasma energy W in Wendelstein~7-X calculated by ASTRA. The ECRH power P is peaked at the axis. It is switched on at the time $t = 0$ and raised by 2 MW per step to a value of 10 MW at $t = 1$ s. The initial value of W is set to 0. 4 MJ. It increases in a series of quasi-stationary states. The final value amounts to 1. 5 MJ. An energy confinement time $\tau_E = 150$ ms is obtained by ASTRA to be compared with values of $\tau_{LGS} = 110$ and $\tau_{LHD} = 70$ ms for the Lackner-Gottardi and LHD scalings, respectively. After the end of the ECRH heating pulse, the plasma energy decays smoothly.

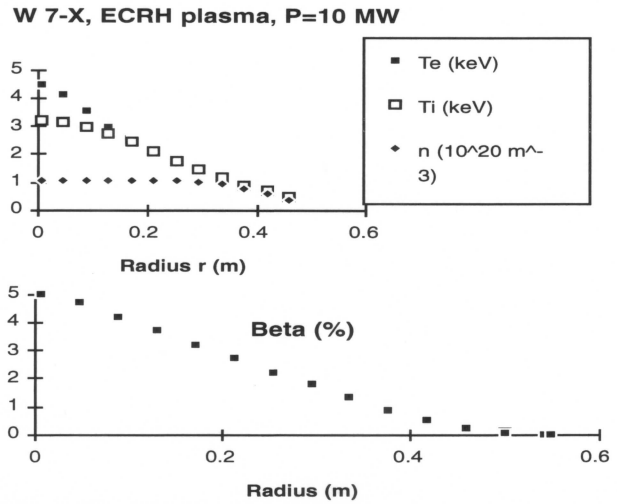

Fig. 2. Stationary profiles of electron and ion temperatures, T_e and T_i, in the final heating phase of Fig. 1. The radial profile of the electron density is fixed in this ASTRA run at a peak value of 10^{20} m^{-3}. The corresponding beta-profile is shown in the lower part of the figure.

[1] Pereverzev, G. V., Yushmanov P. N., et al., IPP-Report 5/42 (1991).
[2] Beidler, C. D., et al., IPP-Report 2/318 (1993).
[3] Kovrizhnykh, L. M., Nuclear Fusion **24** (1984) 435.
[4] IPP Garching Annual Report (1990) 131.

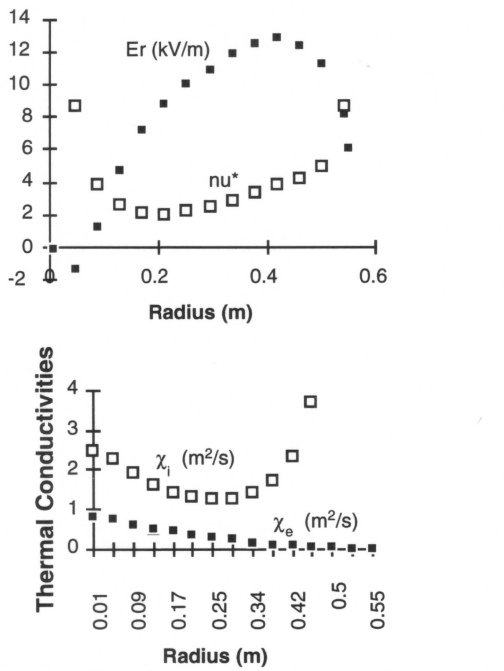

Fig. 3. Profiles of the radial electric field , the normalized collisionality, and the thermal conductivities for the data of Fig. 2.

IPP established at Kharkov

On January 3, 1994, the President of the Ukraine established the Institute of Plasma Physics (IPP) in the *Kharkov Institute of Physics and Technology*, the new national science center. Oleg Pavlichenko was nominated as the Director of this Institute.

Oleg Pavlichenko was graduated from Moscow Physical-Technical Institute. He received his Candidate of Science and Doctor of Science in Physics and Mathematics from Kharkov State University. In 1986 he was awarded the USSR State Prize in Science and Technology for achievements in the development of laser diagnostics.

The IPP employs about 280 people, comprising three divisions:

Stellarator Division (Dr. Eugenij Volkov)
Plasma Theory Division (Dr. Konstantin Stepanov)
Plasmadynamics Division (Dr. Vladimir Tereshin)

The main program issues for the IPP are the development of the stellarator concept and of quasistationary plasma accelerators for fusion and technology applications

The official address if the new institute is:

Institute of Plasma Physics
Academicheskaya St., 1
310108 Kharkov, Ukraine

Oleg Pavlichenko can be reached as follows:

Phone: 007-057-235-6630
FAX: 007-057-235-2664
E-mail:
pavlich%ipp.kharkov.ua@rocket.kharkov.ua

Other E-mail user ids have also been set up:

tereshin (V. Tereshin)
stepanov (K. Stepanov)
volkov (E. Volkov)
shishkin (A. Shishkin)
along (A. Longinov, ICRH group)

For other personnel at Kharkov, use the E-mail postmaster:

ipp%ipp.kharkov.ua@rocket.kharkov.ua